



Cite this: *RSC Adv.*, 2022, 12, 17330

Simple, rapid, and visual electrochemiluminescence sensor for on-site catechol analysis

Suhua Chen,^a Yuanyuan Lei,^b Junrong Xu,^b Yun Yang,^b Yiyi Dong,^b Yanmei Li,^b Haomin Yi,^b Yilong Liao,^b Liyin Chen^b and Yi Xiao^{b,c} 

Environmental pollution caused by aromatic compounds such as catechol (Cat) has become a major issue for human health. However, there is no simple, rapid, and low-cost method for on-site monitoring of Cat. Here, based on ECL quenching mechanism, we develop a simple, rapid and visual mesoporous silica (MSNs)-electrochemiluminescence (ECL) sensor for on-site monitoring of Cat. The mechanism of ECL quenching is due to the interaction between Cat and $\text{Ru}(\text{bpy})_3^{2+}$ and the interactions between the oxidation products of Cat and DBAE. MSNs films with ordered perpendicular mesopore channels exhibit an amplification effect of ECL intensity due to the negatively charged pore channel. There is a good linear relationship between ECL intensity and Cat concentration in the range of 10 ~ 1000 μM with the limit of detection (LOD) of 9.518 μM ($R^2 = 0.99$). The on-site sensor is promising to offer new opportunities for pharmaceuticals analysis, on-site monitoring, and exposure risk assessment.

Received 15th May 2022

Accepted 6th June 2022

DOI: 10.1039/d2ra03067e

rsc.li/rsc-advances

1 Introduction

Environmental pollution caused by aromatic compounds such as catechol (Cat) has become a major issue for human health.^{1–3} Cat is a vital reagent for industry, which is widely used in medicines, dyes, cosmetics, textiles, and the petrochemical industry.⁴ It is a typical phenolic compound that is listed as a potential human carcinogen even at low concentrations.⁵ Cat pose a serious threat to human and environmental health worldwide, and can lead to toxicity to liver, central nervous system and DNA replication.⁶ Therefore, there remains an unmet need to develop a method for determination of Cat concentration for the safety of the environment.

Several analytical techniques including spectrophotometry,⁷ chromatography,⁸ and biosensors^{9–11} are widely used for Cat analysis.¹² These methods offer excellent accuracy and precision,¹³ but suffer from limitations of cumbersome operation, expensive instruments, and time-consuming. Electrochemical techniques (EC) are arousing more and more research interests for Cat analysis,^{14–16} due to their broad dynamic range, excellent temporal controllability, and high sensitivity. A novel 3D aloe-like Au–ZnO nanocomposite was synthesized on ITO substrate

with laccase immobilization, achieving detection of trace Cat in water.¹⁷ An non-enzymatic ZnO WE based strip sensor was developed for the detection of Cat.¹¹ Simultaneous determination of Cat and hydroquinone was achieved using the truncated cube-shaped gold/Prussian blue analogue (Au/PBA) nanocomposites.¹⁸ An amperometric biosensor design based on AuNCs and polyelectrolytes in conjunction with tyrosinase for sensitive detection of Cat.⁴ A biosensor based on the ordered mesoporous carbon nitride material (MCN) to convert the recognition information into a detectable signal with enzyme firstly, which realize the selective detection of Cat and phenol in compost bioremediation samples.² Various nanomaterials have been used for Cat analysis, however, there still remains a need for an ideal nanomaterial for on-site Cat analysis.

Mesoporous silica nanochannels (MSNs) are a film with vertical channel whose pore diameter is 2 ~ 3 nm. Due to MSNs' robust nanostructure and extraordinary properties including high surface area, and controlled pore size, they have attracted considerable attention for the on-site and real-time analysis.^{19–21} Because of the deprotonation of silanol groups with an isoelectric point of 2 ~ 3,^{22,23} MSNs repel the transport of anion while favoring that of cation, and are employed to enrich the luminophores. MSNs membranes can amplify the ECL signal due to electrostatic attraction between silanol groups and $\text{Ru}(\text{bpy})_3^{2+}$. MSNs enhance ECL quenching signal to improve the sensitivity due to the electrostatic interactions. However, the relationship between Cat and ECL activity has yet to be demonstrated. Therefore, we aimed to combine MSNs with ECL to develop a sensor for on-site Cat analysis.

^aHuman Provincial Maternal and Child Health Care Hospital, Changsha 410008, Hunan, China. E-mail: njcpxy4936@163.com

^bKey Laboratory of Study and Discovery of Small Targeted Molecules of Hunan Province, Department of Pharmacy, School of Medicine, Hunan Normal University, Changsha 410013, Hunan, China

^cExperimental Soft Condensed Matter Group, School of Engineering and Applied Sciences, Harvard University, Cambridge, Massachusetts 02138, USA



Here, we developed a simple, rapid and visual MSNs-ECL sensor for on-site Cat analysis. Cat can lead to ECL quenching, and we apply MSNs to amplify the ECL quenching effect. We investigate the effect of $\text{Ru}(\text{bpy})_3^{2+}$ and DBAE on ECL quenching. We study the ultraviolet-visible (UV) spectra, fluorescence (FL) spectra and electrochemical (EC) behavior of ECL system to investigate ECL quenching mechanism. We apply the sensor to determine different concentrations of Cat based on ECL quenching effect. We achieve a simple, rapid and visual method for on-site Cat analysis.

2 Experimental section

2.1. Chemicals and materials

Tris (2,2'-bipyridyl) dichlororuthenium(II) hexahydrate ($\text{Ru}(\text{bpy})_3\text{Cl}_2 \cdot 6\text{H}_2\text{O}$, 99.95%), tetraethyl orthosilicate (TEOS, $\geq 99.0\%$), *N,N*-dibutylethanolamine (DBAE, 99%) and ammonium hydroxide solution (28.0–30.0 wt%) are purchased from Sigma-Aldrich. Hexadecyl trimethyl ammonium bromide (CTAB, 99%) and catechol (Cat, 99%) are purchased from Aladdin. Hydrochloric acid (36.0–38.0 wt%), sodium chloride (NaCl), sodium phosphate dibasic dodecahydrate ($\text{Na}_2\text{HPO}_4 \cdot 12\text{H}_2\text{O}$), sodium dihydrogen phosphate dihydrate ($\text{NaH}_2\text{PO}_4 \cdot 2\text{H}_2\text{O}$), ethanol ($\geq 99.7\%$) and acetone ($\geq 99.5\%$) are obtained from Sinopharm Chemical Reagent Co., Ltd. Ultrapure water ($>18.2 \text{ M}\Omega \text{ cm}^{-1}$) is prepared by Millipore (Milford, MA, USA). ITO glass (square resistance $< 17 \Omega \text{ sq}^{-1}$) is obtained from Kaivo Electronic Components Co., Ltd.

The electrochemical workstation (CHI 660E) is from Shanghai CH Instrument Co., Ltd. Transmission electron microscope (TEM, TecnaiG2 F20) is conducted with a TecnaiG2-F20 transmission electron microscope. Scanning electron

microscope (SEM, SU8010) is performed with a Hitachi-SU8010 scanning electron microscope. Ultra-thin copper grid is obtained from Beijing Zhongke Building Electronic Technology Co., Ltd.

2.2. Preparation of MSNs

ITO glass was cut into $5 \text{ cm} \times 2.5 \text{ cm}$ pieces with a glass cutter and then treated with 1 M NaOH–ethanol solution overnight. It was cleaned ultrasonically by acetone, ethanol, and deionized water for 30 min, and dried under a nitrogen stream. MSNs were synthesized on the surface of ITO electrode by Stöber-solution growth method. 0.16 g CTAB was dissolved in 70 mL deionized water and 30 mL ethanol, then the mixture was stirred to dissolve completely. 10 μL ammonium hydroxide and 80 μL TEOS were added into solution sequentially, and stirred for 10 \sim 15 min. The solution was poured into the box. ITO electrodes were put into the box, and incubated at 60°C for 24 h. The prepared ITO electrodes were rinsed with water, and baked at 100°C overnight. Finally, the prepared ITO electrodes were soaked in 0.1 M HCl–ethanol solution for 15 min, and MSNs-ITO electrodes were obtained after dried under a nitrogen stream.

2.3. Fabrication of MSNs-ECL sensor

As shown in Fig. 1, we fabricate the ECL sensor based on traditional photolithography and wet chemical etching techniques.²⁴ Briefly, we spin-coat the photoresist on the ITO glass substrate ($5.0 \text{ cm} \times 2.5 \text{ cm}$) and then the ITO glass was baked at 110°C for 3 min. Subsequently, the photoresist layer covered ITO glass was exposed to UV light for 4 min under a mask with 18 spots, followed by developing with a 0.7% NaOH solution. After being baked at 110°C , the ITO glass substrate was etched

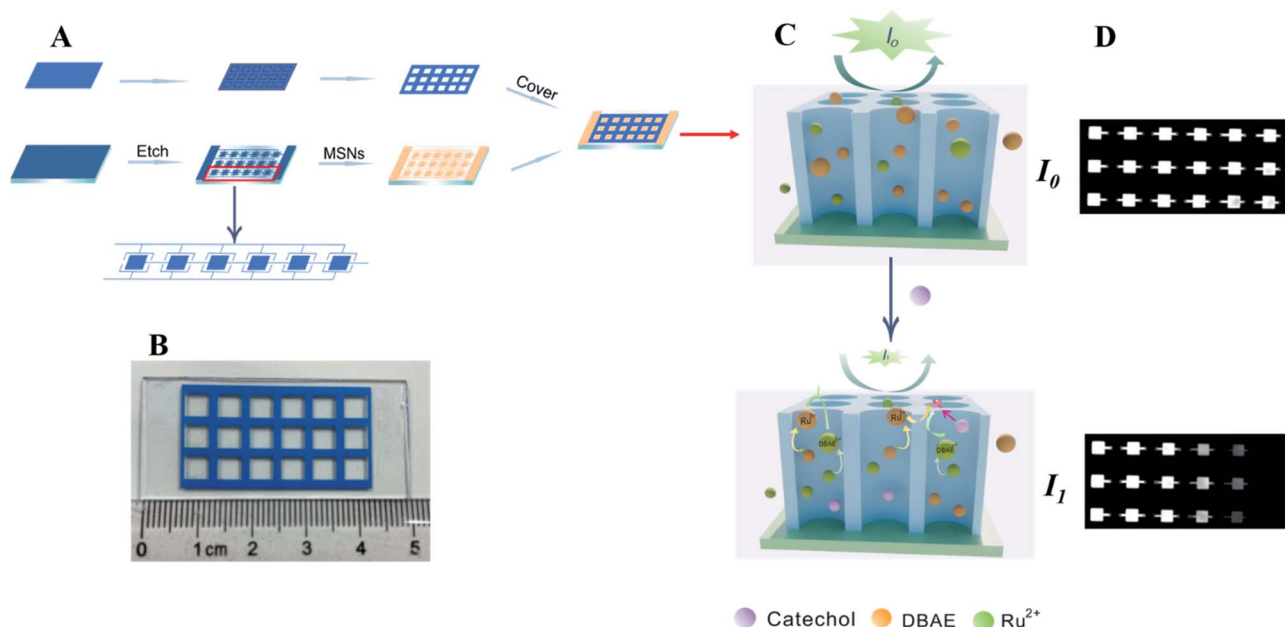


Fig. 1 (A) Fabrication of MSNs-ECL sensor. (B) Photo of ECL sensor. (C) The ECL quenching mechanism. (D) ECL images of different Cat concentrations.



with an aqueous acid solution. Finally, the remaining photoresist was removed by ultrasonication in acetone, and the ITO glass was rinsed with water and dried under an argon stream. MSNs film was prepared onto the patterned ITO electrode by the Stöber-solution growth approach (detailed procedure was shown in 2.3).

A hydrophobic commercial paper (with adhesive tape on one side) was selected and used as the sensor cover. The paper was patterned with Adobe Illustrator software (Adobe Systems, Inc.), and cutted into 18 holes. The sensor was fabricated by simply stacking the paper cover with the MSNs electrode without special bonding technique. These formed microwells were used as reservoirs to align the reaction solutions with the electrode underneath. The working electrode (connecting to one side of the sensor), counter electrode and reference electrode (connecting to the other side of the sensor) make up the three-electrode system. The sensor with 18 detection units enables to detect 18 different samples simultaneously.

We added 10 μL mixture solution of ECL reagent ($\text{Ru}(\text{bpy})_3^{2+}$) and co-reactant (DBAE) to each unit. After applied a certain voltage, ECL was generated. We measure the gray value of the ECL images, and I_0 and I_1 correspond to ECL intensity before and after the addition of Cat, respectively. The ECL quenching efficiency (ΔI) is proportional to the concentration of Cat ($\Delta I = I_0 - I_1$).

2.4. Effect of $\text{Ru}(\text{bpy})_3^{2+}$ or DBAE on ECL quenching

We investigated effect of $\text{Ru}(\text{bpy})_3^{2+}$ concentration on ECL quenching. I_0 of a series of different concentrations of $\text{Ru}(\text{bpy})_3^{2+}$ (10, 100, 500, 1000, 2000, 5000 μM $\text{Ru}(\text{bpy})_3^{2+}$ and 10 μM DBAE) were determined. We investigated effect of DBAE concentration on ECL quenching. I_0 of a series of different concentrations of DBAE (0, 100, 1000, 2000, 5000, 10 000 μM DBAE and 10 μM $\text{Ru}(\text{bpy})_3^{2+}$) were determined. I_1 was determined with the addition of 400 μM Cat.

2.5. Electrochemical and optical measurement

Electrochemical workstation (CHI 660E) and Tanon 4600 Chemiluminescence Imaging System (Tanon Science & Technology Co., Ltd., Shanghai) were applied to collect ECL images. The images were analyzed by Image J. ECL intensity before and after the addition of Cat was I_1 and I_0 ($\Delta I = I_0 - I_1$), respectively. The stock solution of Cat was diluted by 0.1 M PBS (pH = 7.4) into a series of different concentrations solutions (0 μM , 1 μM , 10 μM , 100 μM , 300 μM , 500 μM , and 1000 μM , respectively) with 10 μM $\text{Ru}(\text{bpy})_3^{2+}$. A series of different Cat concentrations solutions with 100 μM DBAE were prepared. A series of different Cat concentrations solutions with 10 μM $\text{Ru}(\text{bpy})_3^{2+}$ and 10 μM DBAE were prepared. 10 μL of each solution was scanned by CVs, which was performed with ITO and MSNs electrode, respectively.

Different solutions (400 μM Cat, 10 μM $\text{Ru}(\text{bpy})_3^{2+}$, 10 μM DBAE, 10 μM $\text{Ru}(\text{bpy})_3^{2+}$ /10 μM DBAE, 10 μM $\text{Ru}(\text{bpy})_3^{2+}$, and 10 μM DBAE/400 μM Cat, 400 μM Ben) were prepared with 0.1 M PBS (pH = 7.4). UV-visible absorption spectra of different solutions were measured.

Different solutions (400 μM Cat, 10 μM $\text{Ru}(\text{bpy})_3^{2+}$, 10 μM DBAE, 10 μM $\text{Ru}(\text{bpy})_3^{2+}$ /10 μM DBAE, 10 μM $\text{Ru}(\text{bpy})_3^{2+}$, and 10 μM DBAE/400 μM Cat) were prepared with 0.1 M PBS (pH = 7.4). Fluorescence spectra of different solutions were measured with an excitation of 452 nm.

3 Results and discussion

3.1. Characterization of MSNs

As shown in Fig. 2, We characterized the morphology of MSNs with SEM and TEM. SEM image shows that the thickness of MSNs is roughly estimated to be 100 nm. TEM image displays the membrane nanochannels with vertical arrangement. As shown in Fig. 2, nanopores have a uniform aperture of 3 nm with an organized distribution and bright spots. And there are no rips or cracks on it. As shown in Fig. 2C, the high-magnification TEM image shows that the pore size is about 2–3 nm, with a high porosity. As shown in Fig. 2D, the cross-sectional TEM shows the nanochannel is vertically aligned.

3.2. Effect of $\text{Ru}(\text{bpy})_3^{2+}$ and DBAE on ECL quenching

As shown in Fig. 3A, ECL quenching efficiency increases with the increasing concentrations of $\text{Ru}(\text{bpy})_3^{2+}$ from 500 μM to 5000 μM . With the increase of $\text{Ru}(\text{bpy})_3^{2+}$ concentrations, ECL quenching effect (ΔI) gradually enhanced. The oxidation product of Cat will quench $\text{Ru}(\text{bpy})_3^{2+}$ via energy transfer. The competition between high concentration of $\text{Ru}(\text{bpy})_3^{2+}$ and DBAE for MSNs will lead to reduced ECL intensity.

Due to the interaction between Cat and DBAE, ECL quenching efficiency (ΔI) raises correspondingly with the increasing DBAE concentration from 10 μM to 10 000 μM , as shown in Fig. 3A. Moreover, the interactions between the

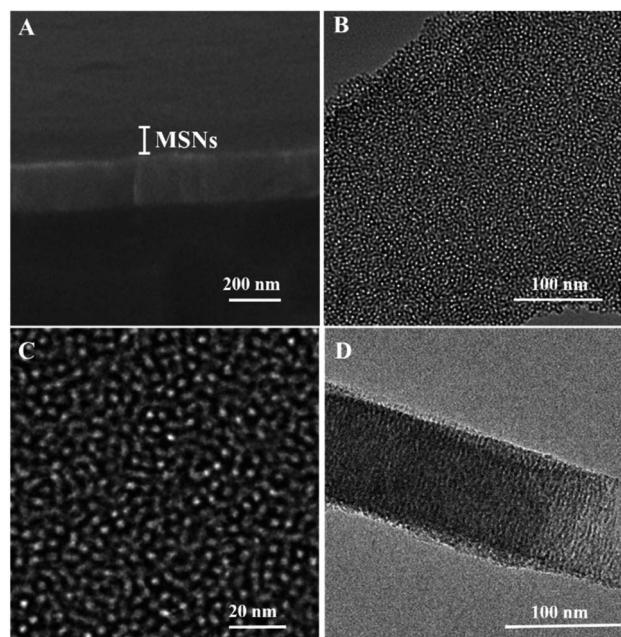


Fig. 2 Morphology of MSNs. (A) SEM and (B) TEM. (C) The high-magnification TEM. (D) The cross-sectional TEM.



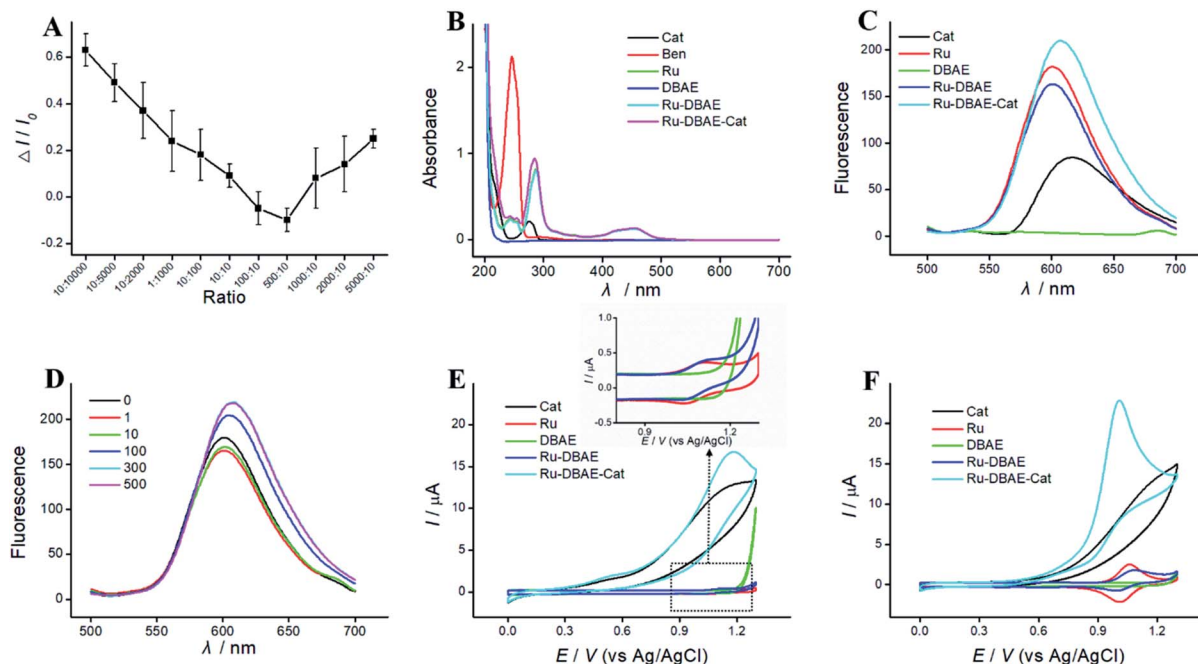


Fig. 3 (A) Effect of $\text{Ru}(\text{bpy})_3^{2+}/\text{DBAE}$ on ECL quenching. Solution contains 400 μM Cat and 10 μM DBAE. (B) UV-vis absorption spectra of different solutions. a. Cat; b. Ben; c. $\text{Ru}(\text{bpy})_3^{2+}$; d. DBAE; e. $\text{Ru}(\text{bpy})_3^{2+}/\text{DBAE}$; f. $\text{Ru}(\text{bpy})_3^{2+}/\text{DBAE}/\text{Cat}$. (C) Fluorescence spectra of different solutions ($\lambda_{\text{exc}} = 452 \text{ nm}$). (D) Fluorescence spectra of $\text{Ru}(\text{bpy})_3^{2+}$, DBAE and different concentrations of Cat. (E) CVs of different solutions at ITO electrode. (F) CVs of different solutions at MSNs electrode. Scan rate: 0.1 V s^{-1} . Error bars represent the standard deviations of three measurements.

oxidation products of Cat and DBAE will consume DBAE and lead to ECL quenching.

3.3. Mechanism of ECL quenching

Fig. 3B shows UV-vis spectra of a series of solutions, including the reaction between $\text{Ru}(\text{bpy})_3^{2+}/\text{DBAE}$ and Cat without electrolysis. We observed that the maximum absorption of Cat was at 290 nm, while the absorption peak didn't change with the addition of $\text{Ru}(\text{bpy})_3^{2+}/\text{DBAE}$. The absorption spectra were just the sum of each component, indicating that simply mixing the three components doesn't generate new compounds without electrolysis. We speculate that electro-oxidation of Cat generates quinones, which can quench $\text{Ru}(\text{bpy})_3^{2+}$ ECL through the electron transfer.²⁵

We investigated FL spectra of a series of solutions to investigate the interaction between the $\text{Ru}(\text{bpy})_3^{2+}/\text{DBAE}$ and Cat without electrolysis.²⁵ FL excitation enables $\text{Ru}(\text{bpy})_3^{2+}$ to generate excited states molecules, but electrolysis is not required for ECL. As shown in Fig. 3C, under the excitation wavelength of 452 nm, $\text{Ru}(\text{bpy})_3^{2+}/\text{DBAE}$ exhibits a peak at 600 nm, while Cat exhibits a peak at 610 nm. Fig. 3D shows FL peak decreases at first, then increases with the increase of Cat concentration. It indicates that Cat may quench $\text{Ru}(\text{bpy})_3^{2+}$ ECL *via* energy transfer.

MSNs films with ordered perpendicular mesopore channels, exhibit amplification effect of ECL intensity due to the negatively charged pore channel, and could adsorb $\text{Ru}(\text{bpy})_3^{2+}$. MSNs is used to amplify ECL signal to improve the sensitivity due to electrostatic attraction between silanol groups and $\text{Ru}(\text{bpy})_3^{2+}$.

After the amplification of ECL intensity, Cat reacts with enriched $\text{Ru}(\text{bpy})_3^{2+}$, and inhibit the amplified ECL intensity. MSNs enhance the ECL quenching signal to improve the sensitivity due to the electrostatic interactions.

3.4. EC behaviors of different ECL systems

To investigate the interaction between Cat and DBAE under electrolysis, CVs were performed (Fig. 3, 4 and 5). As shown in

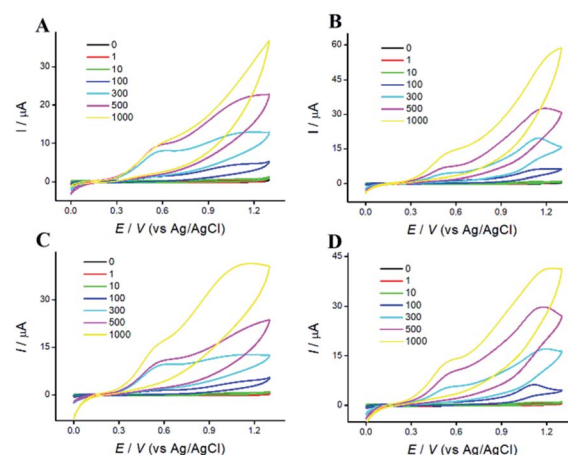


Fig. 4 CVs of different solutions at ITO electrode. (A) Different Cat concentration; (B) different Cat concentration and 10 μM $\text{Ru}(\text{bpy})_3^{2+}$; (C) different Cat concentration and 10 μM DBAE; (D) 10 μM $\text{Ru}(\text{bpy})_3^{2+}$, 10 μM DBAE and different Cat concentrations. Scan rate: 0.1 V s^{-1} .



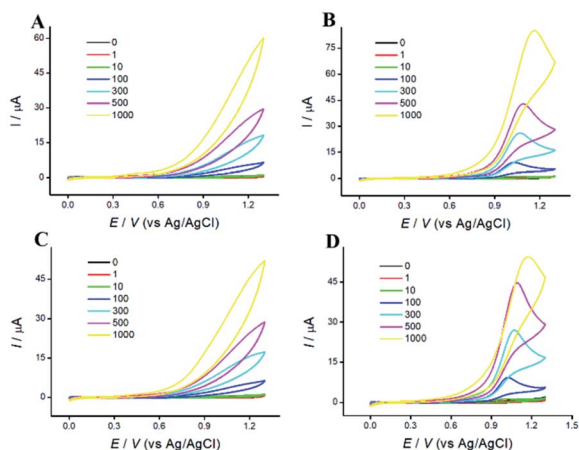


Fig. 5 CVs of different solutions at MSNs electrode. (A) Different Cat concentration; (B) different Cat concentration and 10 μM $\text{Ru}(\text{bpy})_3^{2+}$; (C) different Cat concentration and 10 μM DBAE; (D) 10 μM $\text{Ru}(\text{bpy})_3^{2+}$, 10 μM DBAE and different Cat concentrations. Scan rate: 0.1 V s^{-1} .

Fig. 3, 4 and 5, we observe that both $\text{Ru}(\text{bpy})_3^{2+}$ and DBAE have oxidation–reduction peaks on MSNs electrode, and the peak at 1.15 V is due to the oxidization–reduction reaction of $\text{Ru}(\text{bpy})_3^{2+}$. The voltammetric responses of $\text{Ru}(\text{bpy})_3^{2+}$ and DBAE observed at MSNs electrode are significantly larger than those at ITO electrode. We observed a large peak of $\text{Ru}(\text{bpy})_3^{2+}$ /DBAE at 1.15 V at MSNs electrode, while the current peaks of ITO electrode are at 0.55 V and 1.15 V. The oxidation peak at 0.55 V coincides with the oxidation of Cat. The peak of $\text{Ru}(\text{bpy})_3^{2+}$ /Cat at 1.15 V of MSNs electrode increases with the increment of Cat concentration. Current response at MSNs is as larger than that at ITO, indicating that Cat promoted the oxidization of $\text{Ru}(\text{bpy})_3^{2+}$ and DBAE, and MSNs further amplify the effect. We observed that two peaks of $\text{Ru}(\text{bpy})_3^{2+}$ /DBAE/Cat at MSNs electrode merge into one peak. We infer that there might be an interaction between oxidization of Cat and DBAE, which leads to ECL quenching. MSNs can promote the oxidization of Cat and DBAE.

The ECL quenching mechanism might be explained in two ways. Firstly, the interaction between Cat and $\text{Ru}(\text{bpy})_3^{2+}$ could quench ECL emission of $\text{Ru}(\text{bpy})_3^{2+}$. Cat is oxidized to generate benzoquinone, which can quench the excited-state $\text{Ru}(\text{bpy})_3^{2+}$ via energy transfer. Secondly, the interactions between the

oxidation products of Cat and DBAE can quench the ECL emission. Both direct oxidation of Cat and DBAE takes place at the electrode, and generate the corresponding oxidation products. The interactions between the two oxidation products would consume DBAE and lead to ECL quenching. Hence, the interactions between Cat, $\text{Ru}(\text{bpy})_3^{2+}$ and DBAE lead to ECL quenching.

3.5. Cat analysis

We apply MSNs-ECL sensor for Cat analysis. As shown in Fig. 6, a linear dependence is observed between $\Delta I/I_0$ and Cat concentration in the range from 10 μM to 1000 μM with the detection limit (LOD) of 9.5184 μM ($S/N = 3$). The linear relationship is described as $Y = -0.2920 + 0.0013X$, $R^2 = 0.9906$ (X and Y correspond to the Cat concentration and $\Delta I/I_0$, respectively). As shown in Table 1, our method is comparable to other methods. Our method is simple, and can realize on-site monitoring of Cat. The whole detection process is about 2 min, and 18 samples can be detected simultaneously. The ECL sensor can be applied for different phenols analysis, such as phenol,²³ and acetaminophen.²⁶ The relationship of different phenols and ECL intensity is below.^{27,28} The efficiency of ECL quenching is directly related to the position and number of the substituent on the aromatic ring,²⁸ with meta derivatives displaying the greatest magnitude of quenching, and para derivatives the least. Owing to the ECL activity of a variety of phenols, it is difficult to discriminate between different structures based solely on ECL quenching data. However, our sensor is appropriate for semi-quantitative analysis and determining the total phenol content.

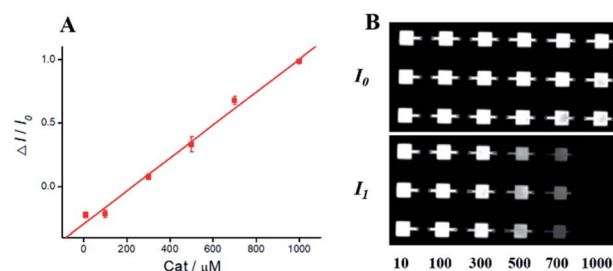


Fig. 6 (A) Calibration curves of different concentrations of Cat. (B) ECL images of different concentrations of Cat. Error bars represent the standard deviations of three measurements.

Table 1 Comparison of analytical performance of Cat

Method	Dynamic range	LOD	Ref.
Polyaniline nanorods	5–100 000 μM	2.1 μM	1
AuNPs/CS@NS/MWCNTS/GCE	1–5000 μM	0.2 μM	6
PEDOT-rGO- Fe_2O_3 -PPO-GC	0.04–62.0 μM	0.007 μM	29
Tyr-AuNC-(PSS-AuNC) ₂ -MPA-AuNP	10 nM–80 μM	0.4 nM	4
<i>E. coli</i> BL21-C230/NPG/GCE	1–500 μM	0.24 μM	30
CdTe QDs-ECL	65–1600 μM	3.754 μM	31
Aloe-like Au–ZnO micro/nanoarrays	75 nM–1100 μM	25 nM	17
Chitosan/alginate polyelectrolytes/tyrosinase sensor	1–300 $\mu\text{g L}^{-1}$	0.86 $\mu\text{g L}^{-1}$	5
Gold/Prussian blue analogue (Au/PBA) nanocomposites	0.2–550 μM	$0.06 \pm 0.001 \mu\text{M}$	18
MSNs-ECL	10–1000 μM	9.5184 μM	This work



The advantage of the sensor is low cost, user-friendly, and portable. LC-MS deals with trace amount measurement of Cat, but our objective is to develop an approach for initial screening of Cat in environment, which is particularly useful for on-site fast Cat screening. Therefore, our sensor can be applied as a rapid screening tool to indicate the exposure risk to Cat. Moreover, the on-site test is of particular value for initial massive sample screening with low requirement of exquisite analytical instrument. Cat exhibit specific and strong signals at the simple, rapid, and low-cost ECL sensor. The Cat sensor is thus suitable for on-site screening, and later on the suspected samples to sensitive laboratory determination.

4 Conclusion

We develop a simple, rapid and visual ECL sensor by combining ECL analysis and nanomaterials, which was used for on-site monitoring of Cat. MSNs films with ordered perpendicular mesopore channels, exhibit amplification effect of ECL intensity due to the negatively charged pore channel, and could block anions and adsorb cations. ECL quenching mechanism includes resonance energy transfer, electron transfer, co-reactant radical quenching, and EC oxidation quenching. The mechanism of ECL quenching might be explained in two ways: (1) Cat is oxidized to yield intermediates, which can quench ECL of the excited state $\text{Ru}(\text{bpy})_3^{2+}$ via electron transfer. (2) The interactions between oxidized radical of DABE and oxidized intermediate radical of Cat would reduce DBAE concentration, which lead to ECL quenching. Moreover, based on the mechanism, we developed a simple, rapid and visual for on-site monitoring of Cat. The on-site sensor based on ECL quenching mechanism is promising to offer new opportunities for pharmaceuticals analysis, on-site monitoring, and exposure risk assessment.

Author contributions

Suhua Chen: conceptualization, methodology, resources, data curation, writing – review & editing. Yuanyuan Lei: visualization, software. Junrong Xu: visualization, software. Yun Yang: software. Yiyi Dong: software. Yanmei Li: software. Haomin Yi: software. Yilong Liao: software. Liyin Chen: writing – review & editing. Yi Xiao: conceptualization, methodology, investigation, writing – original draft, review & editing, funding acquisition, supervision.

Conflicts of interest

The authors declare that they have no known competing financial interests or personal relationships that could have appeared to influence the work reported in this paper.

Acknowledgements

This work was supported by National Natural Science Foundation of China (81803720), Natural Science Foundation of Hunan Province (2019JJ50383), Natural Science Foundation of

Changsha (kq2202256), Huxiang High-Level Talent Innovation Team (2018RS3072), Scientific and Technological Projects for Collaborative Prevention and Control of Birth Defect in Hunan Province (2019SK1012), and Key Grant of Research and Development in Hunan Province (2020DK2002).

References

- 1 V. Gautam, K. P. Singh and V. L. Yadav, Multicomponent Template Effects—Preparation of Highly Porous Polyaniline Nanorods Using Crude Lemon Juice and Its Application for Selective Detection of Catechol, *ACS Sustainable Chem. Eng.*, 2018, **6**(2), 2256–2268.
- 2 Y. Zhou, L. Tang, G. Zeng, J. Chen, Y. Cai, Y. Zhang, G. Yang, Y. Liu, C. Zhang and W. Tang, Mesoporous carbon nitride based biosensor for highly sensitive and selective analysis of phenol and catechol in compost bioremediation, *Biosens. Bioelectron.*, 2014, **61**, 519–525.
- 3 E. Murugan and K. Kumar, Fabrication of $\text{SnS}/\text{TiO}_2@\text{GO}$ Composite Coated Glassy Carbon Electrode for Concomitant Determination of Paracetamol, Tryptophan, and Caffeine in Pharmaceutical Formulations, *Anal. Chem.*, 2019, **91**(9), 5667–5676.
- 4 M. N. Karim, J. E. Lee and H. J. Lee, Amperometric detection of catechol using tyrosinase modified electrodes enhanced by the layer-by-layer assembly of gold nanocubes and polyelectrolytes, *Biosens. Bioelectron.*, 2014, **61**, 147–151.
- 5 R. S. J. Alkasir, M. Ornatska and S. Andreescu, Colorimetric Paper Bioassay for the Detection of Phenolic Compounds, *Anal. Chem.*, 2012, **84**(22), 9729–9737.
- 6 H. Rao, Y. Liu, J. Zhong, Z. Zhang, X. Zhao, X. Liu, Y. Jiang, P. Zou, X. Wang and Y. Wang, Gold Nanoparticle/Chitosan@N,S Co-doped Multiwalled Carbon Nanotubes Sensor: Fabrication, Characterization, and Electrochemical Detection of Catechol and Nitrite, *ACS Sustainable Chem. Eng.*, 2017, **5**(11), 10926–10939.
- 7 C. Liu, J. Hu, S. Biswas, F. Zhu, J. Zhan, G. Wang, C.-H. Tung and Y. Wang, Surface-Enhanced Raman Scattering of Phenols and Catechols by a Molecular Analogue of Titanium Dioxide, *Anal. Chem.*, 2020, **92**(8), 5929–5936.
- 8 S. R. Wallenborg, L. Nyholm and C. E. Lunte, End-Column Amperometric Detection in Capillary Electrophoresis: Influence of Separation-Related Parameters on the Observed Half-Wave Potential for Dopamine and Catechol, *Anal. Chem.*, 1999, **71**(3), 544–549.
- 9 L.-J. Zhao, R.-C. Qian, W. Ma, H. Tian and Y.-T. Long, Electrocatalytic Efficiency Analysis of Catechol Molecules for NADH Oxidation during Nanoparticle Collision, *Anal. Chem.*, 2016, **88**(17), 8375–8379.
- 10 B. Wolfrum, M. Zevenbergen and S. Lemay, Nanofluidic Redox Cycling Amplification for the Selective Detection of Catechol, *Anal. Chem.*, 2008, **80**(4), 972–977.
- 11 A. Maikap, K. Mukherjee, B. Mondal, N. Mandal and A. K. Meikap, A novel non-enzymatic zinc oxide thin film based electrochemical recyclable strip with device interface for quantitative detection of catechol in water, *Biosens. Bioelectron.*, 2019, **128**, 32–36.



- 12 X. Liu, J. Yang, J. Cheng, Y. Xu, W. Chen and Y. Li, Facile preparation of four-in-one nanozyme catalytic platform and the application in selective detection of catechol and hydroquinone, *Sens. Actuators, B*, 2021, **337**, 129763.
- 13 S. H. DuVall and R. L. McCreery, Control of Catechol and Hydroquinone Electron-Transfer Kinetics on Native and Modified Glassy Carbon Electrodes, *Anal. Chem.*, 1999, **71**(20), 4594–4602.
- 14 C. Ma, Y. Cao, X. Gou and J. J. Zhu, Recent Progress in Electrochemiluminescence Sensing and Imaging, *Anal. Chem.*, 2020, **92**(1), 431–454.
- 15 A. Jones, L. Dhanapala, R. N. T. Kankanamage, C. V. Kumar and J. F. Rusling, Multiplexed Immunosensors and Immunoarrays, *Anal. Chem.*, 2020, **92**(1), 345–362.
- 16 W. Lv, H. Ye, Z. Yuan, X. Liu, X. Chen and W. Yang, Recent advances in electrochemiluminescence-based simultaneous detection of multiple targets, *TrAC, Trends Anal. Chem.*, 2020, **123**, 115767.
- 17 T. Liu, Q. Zhao, Y. Xie, D. Jiang, Z. Chu and W. Jin, In situ fabrication of aloe-like Au–ZnO micro/nanoarrays for ultrasensitive biosensing of catechol, *Biosens. Bioelectron.*, 2020, **156**, 112145.
- 18 D. Jiang, J. Pang, Q. You, T. Liu, Z. Chu and W. Jin, Simultaneous biosensing of catechol and hydroquinone via a truncated cube-shaped Au/PBA nanocomposite, *Biosens. Bioelectron.*, 2019, **124–125**, 260–267.
- 19 F. Yan, Y. He, L. Ding and B. Su, Highly Ordered Binary Assembly of Silica Mesochannels and Surfactant Micelles for Extraction and Electrochemical Analysis of Trace Nitroaromatic Explosives and Pesticides, *Anal. Chem.*, 2015, **87**(8), 4436–4441.
- 20 Z. Teng, G. Zheng, Y. Dou, W. Li, C. Y. Mou, X. Zhang, A. M. Asiri and D. Zhao, Highly ordered mesoporous silica films with perpendicular mesochannels by a simple Stober-solution growth approach, *Angew. Chem., Int. Ed. Engl.*, 2012, **51**(9), 2173–2177.
- 21 Y. Xiao, S. Chen, G. Zhang, Z. Li, H. Xiao, C. Chen, C. He, R. Zhang and X. Yang, Simple and rapid nicotine analysis using a disposable silica nanochannel-assisted electrochemiluminescence sensor, *Analyst*, 2020, **145**(14), 4806–4814.
- 22 Y. Xiao, L. Xu, P. Li, X.-C. Tang and L.-W. Qi, A simple microdroplet chip consisting of silica nanochannel-assisted electrode and paper cover for highly sensitive electrochemiluminescent detection of drugs in human serum, *Anal. Chim. Acta*, 2017, **983**, 96–102.
- 23 Y. Xiao, S. Chen, S. Zhang, G. Wang, H. Yi, G.-Z. Xin and X. Yang, Mesoporous silica-mediated controllable electrochemiluminescence quenching for immunosensor with simplicity, sensitivity and tunable detection range, *Talanta*, 2021, **231**, 122399.
- 24 D. C. Duffy, J. C. McDonald, O. J. A. Schueller and G. M. Whitesides, Rapid Prototyping of Microfluidic Systems in Poly(dimethylsiloxane), *Anal. Chem.*, 1998, **70**(23), 4974–4984.
- 25 H. Sha, Y. Zhang, Y. Wang, H. Ke, X. Xiong, H. Xue and N. Jia, Electroluminescent aptasensor based on RuSiO₂ nanoparticles for detection cytochrome c using ferrocene as quenching probe, *Biosens. Bioelectron.*, 2019, **132**, 203–209.
- 26 Y. Xiao, G. Wang, H. Yi, S. Chen, Q. Wu, S. Zhang, K. Deng, S. Zhang, Z.-Q. Shi and X. Yang, Electrogenated chemiluminescence of a Ru (bpy) ₃ ²⁺/arginine system: a specific and sensitive detection of acetaminophen, *RSC Adv.*, 2022, **12**(5), 3157–3164.
- 27 B. Huang, X. Zhou, Z. Xue and X. Lu, Electrochemiluminescence quenching of tris (2, 2'-bipyridyl) ruthenium, *TrAC, Trends Anal. Chem.*, 2013, **51**, 107–116.
- 28 J. McCall and M. M. Richter, Phenol substituent effects on electrogenerated chemiluminescence quenching, *Analyst*, 2000, **125**(3), 545–548.
- 29 V. Sethuraman, P. Muthuraja, J. Anandha Raj and P. Manisankar, A highly sensitive electrochemical biosensor for catechol using conducting polymer reduced graphene oxide–metal oxide enzyme modified electrode, *Biosens. Bioelectron.*, 2016, **84**, 112–119.
- 30 Z. Liu, Y. Zhang, C. Bian, T. Xia, Y. Gao, X. Zhang, H. Wang, H. Ma, Y. Hu and X. Wang, Highly sensitive microbial biosensor based on recombinant Escherichia coli overexpressing catechol 2,3-dioxygenase for reliable detection of catechol, *Biosens. Bioelectron.*, 2019, **126**, 51–58.
- 31 X. Liu, H. Jiang, J. Lei and H. Ju, Anodic Electrochemiluminescence of CdTe Quantum Dots and Its Energy Transfer for Detection of Catechol Derivatives, *Anal. Chem.*, 2007, **79**(21), 8055–8060.

